ISBN: 978-3-95450-234-9 ISSN: 2673-5504 doi:10.18429/JACoW-SRF2023-MOPMB029

EXPLORING THE DYNAMICS OF TRANSVERSE INTER-PLANAR COUPLING IN THE SUPERCONDUCTING SECTION OF THE PIP-II LINAC*

Abhishek Pathak†, Fermi National Accelerator Laboratory, Batavia, IL, USA
Eduard Pozdeyev, Thomas Jefferson National Accelerator Facility, Newport News, VA, USA

Abstract

This study investigates the crucial role that an accurate understanding of inter-planar coupling in the transverse plane plays in regulating charged particle dynamics in a high-intensity linear accelerator and minimizing foil/septum impacts during injection from the linac to a ring. We performed an in-depth analysis for the emergence and evolution of transverse inter-planar coupling through multiple active lattice elements, taking into account space charge and field nonlinearities in the superconducting section of the PIP-II linac. The article compares various analytical, numerical, and experimental techniques for measuring transverse coupling using beam and lattice matrices and provides insight into effective strategies for its mitigation prior to ring injection

INTRODUCTION

The Fermilab PIP-II [1] upgrade aims to support the Deep Underground Neutrino Experiment (DUNE) at LBNF by accelerating a high-intensity H^- CW beam to 800 MeV, with 1.6 MW power output. Ensuring optimal performance involves careful control of emittance blow-up, halo growth, and transmission loss. Among various challenges, transverse inter-planar coupling [2] can cause significant emittance blow-up and beam loss through the creation of ellipticity [3] in the transverse particle density distribution.

This article delves into factors such as space charge non-linearity and off-diagonal terms in the lattice elements that contribute to the transverse inter-planar coupling. It subsequently juxtaposes different measurement techniques for quantifying the extent of inter-planar coupling in the high beta section of the linac beam. Lastly, it advocates for potential techniques to abate the coupling terms from the beam matrix prior to injection into the booster.

SPACE CHARGE AND INTER-PLANAR COUPLING

In the study of non-relativistic charged particle beams' dynamics in high-intensity accelerators, the nonlinear space-charge forces are pivotal as they degrade the beam's quality and introduce inter-planar coupling. Our Particle-in-Cell simulations via the TraceWin code, employing Gaussian, parabolic, water-bag, and KV particle density distributions, were performed to analyze the impact of these forces on transverse beam coupling. We utilized a drift of 1.5 m, devoid of any external fields, to measure the inter-planar coupling, and introduced a coupling parameter Σ defined as $\sqrt{\sigma_{1,3}^2 + \sigma_{1,4}^2 + \sigma_{2,3}^2 + \sigma_{2,4}^2}$, where $\sigma_{i,j}$ are off-diagonal terms in the beam's sigma matrix.

The study reveals a non-linear rise in the coupling parameter,

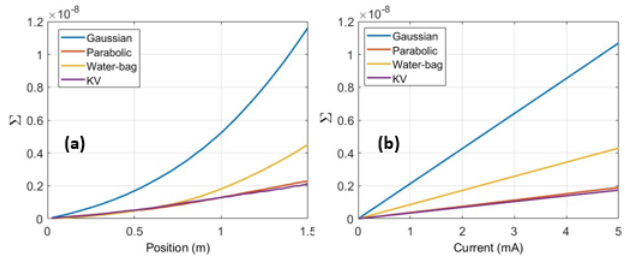

Figure 1: (a) Depiction of the variation in the inter-planar coupling term along a drift, stemming from initial particle density distributions with varying degrees of space charge nonlinearity. (b) Display of the fluctuation in the inter-planar coupling term in relation to beam current, associated with initial particle density distributions subject to various levels of space charge nonlinearity.

Σ, as the beam propagates through the drift space, influenced by the non-linearity in the space-charge field. Moreover, Σ linearly grows with the beam current, independent of space-charge non-linearity, yet the growth rate is influenced by the initial particle distribution. Figures 1(a) and 2(b) illustrate the variation of Σ across a 1.5 m drift space and its relation to the beam current, highlighting the significant role of space-charge effects in high-intensity accelerators. The correlation of Σ with beam radius was explored using an 800 MeV, 5 mA H^- beam. We computed Σ for particles within varying transverse radii from the core to the tail. Figure 2(a) shows y-integrated density along x, while Fig. 2(b) displays Σ variation from the beam's core to the tail. Within a 2 mm radius, Σ remains fairly constant. However, moving outwards, Σ nonlinearly decreases - most steeply for the KV distribution and least for Gaussian. Thus, tail region particles in a non-linear density distribution significantly influence x-y beam coupling.

LATTICE ELEMENTS AND INTRA-PLANAR COUPLING

Utilizing field maps across the PIP-II lattice, we linearized the motion equations of charged particles in RF fields to derive transfer matrices. This included the consideration of

* This manuscript has been authored by Fermi Research Alliance, LLC under Contract No. DE-AC02-07CH11359 with the US Department of Energy, Office of Science, Office of High Energy Physics.
† abhishek@fnal.gov

ISBN: 978-3-95450-234-9 ISSN: 2673-5504 doi:10.18429/JACoW-SRF2023-MOPMB029

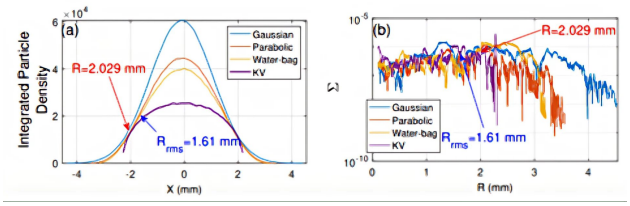

Figure 2: (a) X-axis cross-sectional representation of the particle density distribution at the conclusion of a 1.5 m drift. (b) Plot showcasing the variation of the coupling parameter Σ as calculated based on the particles situated within a specified transverse radius r, presented as a function of r on a semi-logarithmic scale.

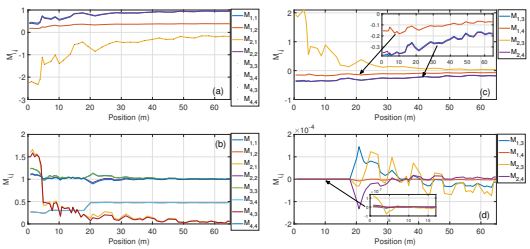

Figure 3: The diagonal (a, c) and off-diagonal (b, d) elements derived from the cavity and solenoid transfer matrices, depicted over the HWR and SSR portions of the PIP-II linac.

the momentum evolution of charged particles with charge 'q' and mass 'm' in Cartesian coordinates:

$$\begin{aligned}\frac{dx'}{ds} =& \frac{q}{\beta_z^2 \gamma mc^2}\left(E_{x,0} - \beta_z.c.B_{y,0}\right) - E_{z,0}.x' + \beta_z c.B_{z,0}.y' \\ &- \left((2-\beta_z^2).E_{y,0} + \beta_z c.B_{x,0}\right).\delta \\ &+ \left(\frac{\partial E_y}{\partial x} + \beta_z c\frac{\partial B_x}{\partial x}\right).x + \left(\frac{\partial E_y}{\partial y} - \beta_z c\frac{\partial B_x}{\partial y}\right).y \\ &+ \left(\frac{\partial E_x}{\partial z} - \beta_z c\frac{\partial B_y}{\partial z}\right).z, \end{aligned} \tag{1}$$

$$\begin{aligned}\frac{dx'}{ds} =& \frac{q}{\beta_z^2 \gamma mc^2}\left(E_{y,0} - \beta_z.c.B_{x,0}\right) - E_{z,0}.y' - \beta_z c.B_{z,0}.x' \\ &- \left((2-\beta_z^2).E_{x,0} + \beta_z c.B_{y,0}\right).\delta \\ &+ \left(\frac{\partial E_x}{\partial x} - \beta_z c\frac{\partial B_y}{\partial x}\right).x + \left(\frac{\partial E_x}{\partial y} - \beta_z c\frac{\partial B_y}{\partial y}\right).y \\ &+ \left(\frac{\partial E_y}{\partial z} - \beta_z c\frac{\partial B_x}{\partial z}\right).z. \end{aligned} \tag{2}$$

Integration of Eqs. (1) and (2) across each lattice component results in transfer matrices defined as a function of pertinent parameters such as beam energy, synchronous phase, accelerating gradients, and solenoid field, all of which constitute the optimized PIP-II lattice. The resulting matrix components are depicted in Fig. 3.

Our comprehensive analysis indicates that the coupling elements from the individual constituents are of a negligible magnitude. Rather, it is the synergistic interaction between the cavities and the solenoid under the influence of space charge forces that gives rise to transverse coupling within the beam. As the beam energy escalates, the space charge forces in conjunction with RF defocusing decline, consequently causing regions of low energy such as the HWR and SSR-1 to initiate x-y splitting within the beam.

QUANTIFICATION OF TRANSVERSE INTER-PLANAR COUPLING

To effectively manage transverse inter-planar coupling before the beam is introduced into the booster, suitable beam diagnostics such as a wire scanner should be appropriately placed. This positioning allows the reconstruction of the beam sigma matrix and hence facilitates the identification of the respective coupling terms.

The transverse beam matrix comprises ten independent elements, among which, three outline the x-x' phase space, another three specify the y-y' phase space, and the remaining four elements quantify the coupling between the x-x' and y-y' planes. Given the transformation of the beam sigma matrix from one lattice point to another ($\sigma_f = T\sigma_i T^T$), ten measurements are necessary for the complete reconstruction of the initial beam matrix. Consequently, this enables the application of suitable measures to counterbalance the coupling terms in the beam.

If we adopt wire scanners with three wires, there exist two feasible algorithms to secure the desired measurements. The first strategy necessitates the placement of four such wire scanners across four different locations, which will provide twelve measurements (an overdetermined system). Alternatively, the second approach requires the installation of a single wire scanner, for which measurements are obtained under four distinct settings of the lattice optics. We undertook numerical modeling for both the aforementioned algorithms, with the resulting comparison depicted in Table 1. As indicated in the Table 1, both approaches yield similar results, establishing their equal reliability. However, Scheme II only necessitates the use of a single wire-scanner. This considerably simplifies the process of identifying the coupling terms, thereby making it the more pragmatic option when dealing with the determination and compensation of the off-diagonal terms in the beam matrix.

DECOUPLING TRANSVERSE INTER-PLANAR COUPLING

Adopting one of the proposed methodologies enables the reconstruction of the beam matrix at the entry point. The quantification of inter-planar coupling strength is achieved by examining the off-diagonal terms in the reconstructed beam matrix. To negate x-y coupling, the coupling metrics σ_{13}, σ_{14}, σ_{23}, and σ_{24} should approximate zero.

ISBN: 978-3-95450-234-9 ISSN: 2673-5504 doi:10.18429/JACoW-SRF2023-MOPMB029

Table 1: Comparison of the Two Schemes

	From Distribution	Scheme-I	Scheme-I % Difference	Scheme-II	Scheme-II % Difference
σ_{13}	3.3121177×10^{-7}	3.46738×10^{-7}	4.69	3.14325×10^{-7}	-5.1
σ_{14}	4.6752332×10^{-7}	4.81698×10^{-7}	3.03	4.5625×10^{-7}	-2.41
σ_{23}	4.9233216×10^{-7}	4.81001×10^{-7}	-2.35	4.82975×10^{-7}	-1.9
σ_{24}	3.7760945×10^{-8}	3.65852×10^{-8}	-3.11	3.76652×10^{-8}	-0.25

$$\sigma_{13,B} = M_{11}M_{33}\sigma_{13} + M_{11}M_{34}\sigma_{14} + M_{12}M_{33}\sigma_{23} + M_{12}M_{34}\sigma_{24},$$
$$\sigma_{14,B} = M_{11}M_{43}\sigma_{13} + M_{11}M_{44}\sigma_{14} + M_{12}M_{43}\sigma_{23} + M_{12}M_{44}\sigma_{24},$$
$$\sigma_{23,B} = M_{21}M_{33}\sigma_{13} + M_{21}M_{34}\sigma_{14} + M_{22}M_{33}\sigma_{23} + M_{22}M_{34}\sigma_{24},$$
$$\sigma_{24,B} = M_{21}M_{43}\sigma_{13} + M_{21}M_{44}\sigma_{14} + M_{22}M_{43}\sigma_{23} + M_{22}M_{44}\sigma_{24}.$$

These expressions can be succinctly represented in matrix form:

$$\Sigma = \mathbf{A}\Sigma_0 \tag{3}$$
$$\mathbf{A}^T\Sigma = \mathbf{A}^T\mathbf{A}\Sigma_0 \tag{4}$$

which further implies:

$$\Sigma_0 = (\mathbf{A}^T\mathbf{A})^{-1}\mathbf{A}^T\Sigma. \tag{5}$$

Upon determination of the initial coupling terms, the subsequent expression can be used:

$$(\mathbf{A}^T\mathbf{A})^{-1}\mathbf{A}^T\Sigma = \mathbf{0}. \tag{6}$$

This allows the determination of transfer matrix elements that lead to an uncoupled beam in the transverse plane.

$$(\mathbf{A}^T\mathbf{A})^{-1}\mathbf{A}\Sigma = \mathbf{0} \tag{7}$$

Solving this equation yields the off-diagonal terms in the transfer matrix necessary to negate the initial coupling using skew quadrupoles. The PIP-II linac strategically integrates four skew quadrupoles within the HB-650 section. This design configuration is aimed at counteracting instances where the transverse interplanar coupling is not adequately compensated within the HWR and SSR sections of the linac. In our current investigation, we have intentionally overestimated the coupling term (10^{-7}) and employed the outlined algorithm to effectively alleviate it. This process involves the precision tuning of matrix elements corresponding to the four skew quadrupoles. The results shown in Table 2 strongly indicate that the skew quadrupoles strategically positioned within the high-energy section of the linac are sufficiently capable of compensating for any potential transverse inter-planar coupling within the beam.

Table 2: Mitigation of the Transverse Interplanar Coupling Terms via Skew Quadrupoles

Coupling Terms	Before Compensation	After Compensation
σ_{13}	7.14325×10^{-8}	6.1536×10^{-14}
σ_{14}	4.5625×10^{-7}	2.2534×10^{-15}
σ_{23}	4.82975×10^{-7}	1.6732×10^{-14}
σ_{24}	3.76652×10^{-8}	5.9538×10^{-13}

CONCLUSION

This study highlights the significance of accurate knowledge of transverse inter-planar coupling in the beam in a high-intensity accelerator like PIP-II. Our study shows a nonlinear increase in the coupling terms as the beam propagates under the influence of space-charge forces, and the degree of nonlinearity is driven by the nonlinearity in the space-charge field.

Our study also shows that individual cavities and the solenoid have an insignificant contribution to the x-y splitting of the beam, and it is the combined role of the period in the presence of nonlinear space-charge forces that increases the transverse coupling as the beam propagates along the linac.

Here we also propose and compare two possible approaches to quantify the transverse coupling terms using wire scanners and demonstrate that they produce similar results, with a deviation from the real value within 6%.

Finally, we demonstrate the efficacy of the four skew quadrupoles strategically placed in the high beta section of the PIP-II linac in mitigating the maximum possible transverse inter-planar coupling in the beam. We show that an optimal configuration of these skew quadrupoles can bring down the coupling term from the order of 10^{-7} to 10^{-15}.

REFERENCES

[1] V. Lebedev, "The PIP-II reference design report", FNAL, IL, USA, FERMILAB-DESIGN-2015-011607162, 2015.

[2] E. Prat and M. Aiba, "Four-dimensional transverse beam matrix measurement using the multiple-quadrupole scan technique", *Phys. Rev. Spec. Top. Accel. Beams*, vol. 17, p. 052801, 2014. doi:10.1103/PhysRevSTAB.17.052801

[3] A. Pathak and E. Pozdeyev, "Optimization of Superconducting Linac for Proton Improvement Plan-II (PIP-II)", in *Proc. NAPAC'22*, Albuquerque, NM, USA, Aug. 2022, pp. 132–135. doi:10.18429/JACoW-NAPAC2022-MOPA36